Chapter 5

Improving vertical charge transport in organic Schottky diodes via Interface engineering of large-area conducting polymer thin films fabricated on hydrophilic liquid surface of tunable surface energy

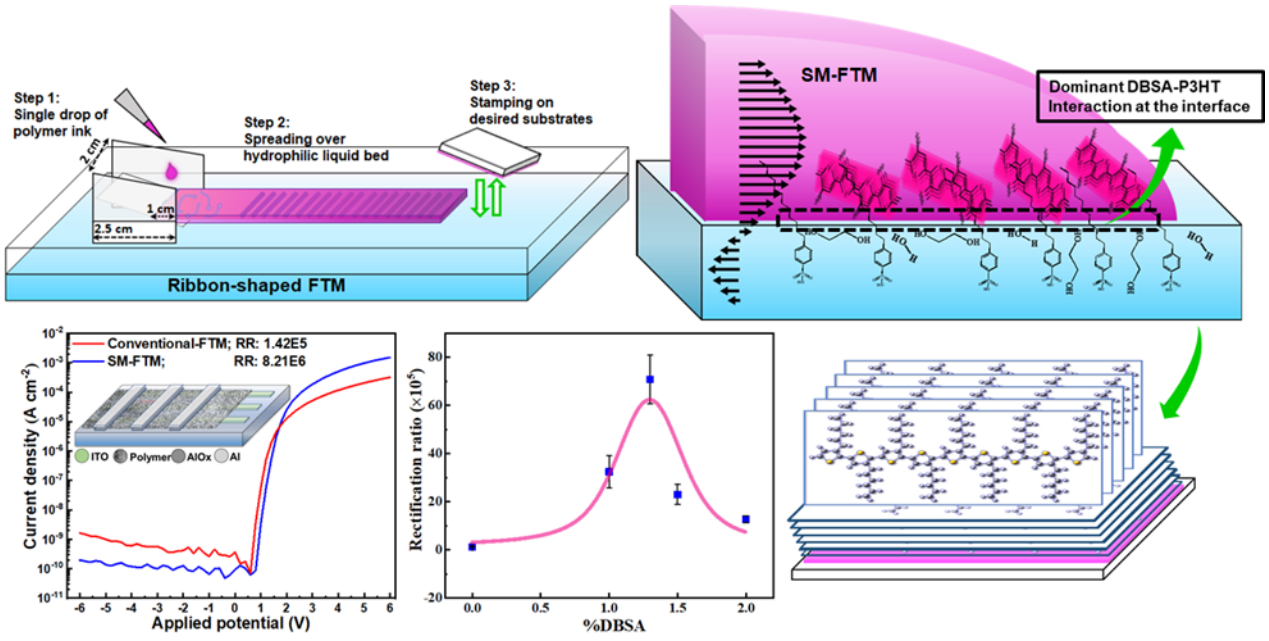

5.1.Introduction

Solution processability, easy functionalization, lightweight, and mechanical flexibility make semiconducting conducting polymers (CPs) suitable for vast applications- starting from electronic and photovoltaic to gas sensors, energy harvesting, electrochemical and bio-related applications[2,143–145]. In the last few decades, among the organic electronic devices, organic field-effect transistors (OFET), rectifiers, electro-chromic devices (PEC), thermoelectric generators, organic light-emitting diodes (OLED), polymer solar cells, etc. have been fabricated and extensively researched by various groups worldwide. Among them, only a few devices like PEC and PLED found their way out from the laboratory level to industries owing to exceptional cost-to-performance ratio [6,7]. Other electronic devices still lack performance, stability, reproducibility, and an operational lifetime to compete with commercially available silicon-based devices.

In terms of mobility that determines the processing speed of a device, CPs are much behind the highly crystalline silicon because of their relatively slow carrier hopping mechanism. However, in various applications where carrier mobility is not the key requirement, like diode rectifiers, low-cost solution processable organic film fabrication techniques can be preferred. Moreover, huge efforts are being put in by many research groups to develop these techniques to harness optimum device performance [21]. That is why organic-based Schottky barrier diodes (SBDs) with various applications like printed radio frequency identification (RFID) tags, [146] wireless communications, [147] energy harvesting devices (rectenna), [148] etc. gained much interest in the past decade. High-speed organic SBDs require high forward bias current density for rapid charging of load circuits, negligible reverse saturation current density to minimize load capacitor charge leakage in time of reverse bias half cycle, and effectively high Schottky barrier to enhance the rectification ratio (RR). These requirements can be fulfilled by injection-efficient contacts,

improving the bulk quality of the active layer, and minimizing interfacial contact resistance (R_c). The presence of trap states, surface dangling bonds, electrode-semiconductor energy level mismatch and band bending contribute to R_c, while the film crystallinity and type of molecular arrangement dictate the bulk resistance, R_b. Even after the right choice of electrode material whose Fermi level matches well with the semiconductor HOMO (highest occupied molecular orbital) level, the interfacial charge-double layer can introduce an injection barrier [81]. Many innovative strategies and thin-film fabrication technologies have been developed in this regard, like hybrid organic−inorganic heterojunction formation, [149] substrate surface treating with polar molecule, [150] incorporations of a buffer layer,[151] composite formations with 2D filler, [152] use of polymer fibril structure, [153] etc. But except for very few cases of small molecule-SBD where ultra-high vacuum deposition is also needed, [154,155] there still exists much difficulty in achieving high RR for solution-processed semiconducting polymer-based SBDs.

Now, it has been well established that the oriented CPs show charge transport anisotropy, [117] where the molecular backbone direction provides the highest carrier mobility, then the π-π stacking direction, and lastly, the non-conducting alkyl side-chain stacking which resists carrier mobility the most. Thus, using a 'face-on' type molecular stacking for the fabrication of an out-of-plane diode structure can help achieve high-performing SBD. Although an 'end-on' type molecular packing, where the polymer backbone chains lie perpendicular to the film plane, should provide the highest mobility in this regard, this type of packing is rarely found without end-functionalization because of its highly unstable arrangement [156,157]. In contrast, 'face-on' stacking is achievable with the friction transferred method and biaxial straining approach, etc. [158,159]. But biaxial straining is a much more complex multistep method, and the friction transferred technique is not suitable for industrial-level scaling. In collaboration with Japanese researchers, our group has also

developed a much facile technique, the Floating film Transfer Method (FTM), [57] suitable for highly oriented, [67] large-area [67,160,161] thin polymeric film fabrication. As FTM provides thin solid films floating on a hydrophilic liquid substrate, layer-by-layer deposition [68] is also possible through it. However, it has been found from previous investigations [57,124,162] that major polythiophene derivatives like rr-P3HT form highly 'edge-on' type molecular stacking in the films while processed through FTM, which will be beneficial for OFETs, but not for SBDs. Recently, Xin Gao et al. [163] proposed a new strategy to enhance the functionality and performance of flexible piezocomposites by designing delivery paths, which motivated us to do interfacial engineering while preparing large-area films through FTM.

In this manuscript, we have used Dodecylbenzene Sulfonic Acid (DBSA) in the hydrophilic liquid base, which should facilitate the interaction between rr-P3HT alkyl side-chains and the long hydrophobic part of DBSA to form a 'face-on' type stacking. To confirm the molecular rearrangement in P3HT thin films and their effect on crystalline domains and electronic band structure, we have examined those films through multiple characterization techniques like out-of-plane and in-plane GIXD, HR-TEM, UV-vis spectroscopy, AFM, contact angle measurement, and cyclic voltammetry. Furthermore, we have studied the effect of molecular rearrangement on device performance through multiple SBDs and the RR (8.2×10^6) is found to be one of the best results reported till now. Then, to get a clear understanding of the origin of this molecular rearrangement through interfacial engineering, we have analyzed the dynamics of polymer spreading over hydrophilic liquid subphase and developed a model using lubrication theory and thin-film dynamics which will be helpful for comprehending the fundamentals.

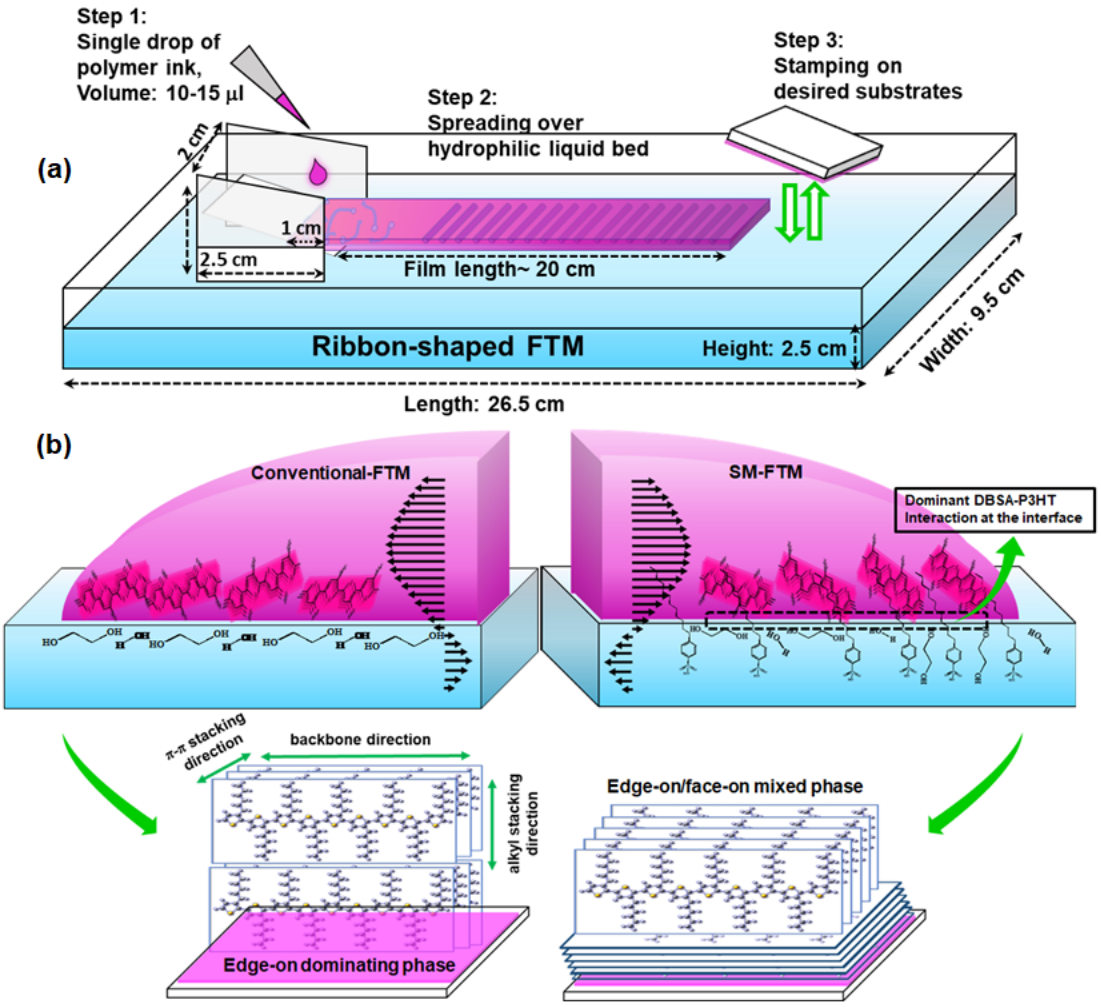

Figure 5.1 (a) Ribbon-shaped FTM process, (b) Evolution of molecular arrangements in P3HT films formed through both conventional- and SM-FTM.

5.2.Results and Discussion

5.2.1. Film characterizations

Previous studies on crystalline fractions of semicrystalline poly(alkylthiophene)s evidenced that, two types of molecular stacking are very common in P3HT, where π-π stacking lies parallel (‘edge-on’) and perpendicular (‘face-on’) to the film surface. In the orthogonal packing of planar P3HT chains, the side-chain interdigitation direction (*h*00), is globally recognized as ‘a’-axis, π-π stacking direction (0*k*0) as ‘b’-axis and the intramolecular backbone as ‘c’-axis [158]. Thus, if the molecular arrangement present in

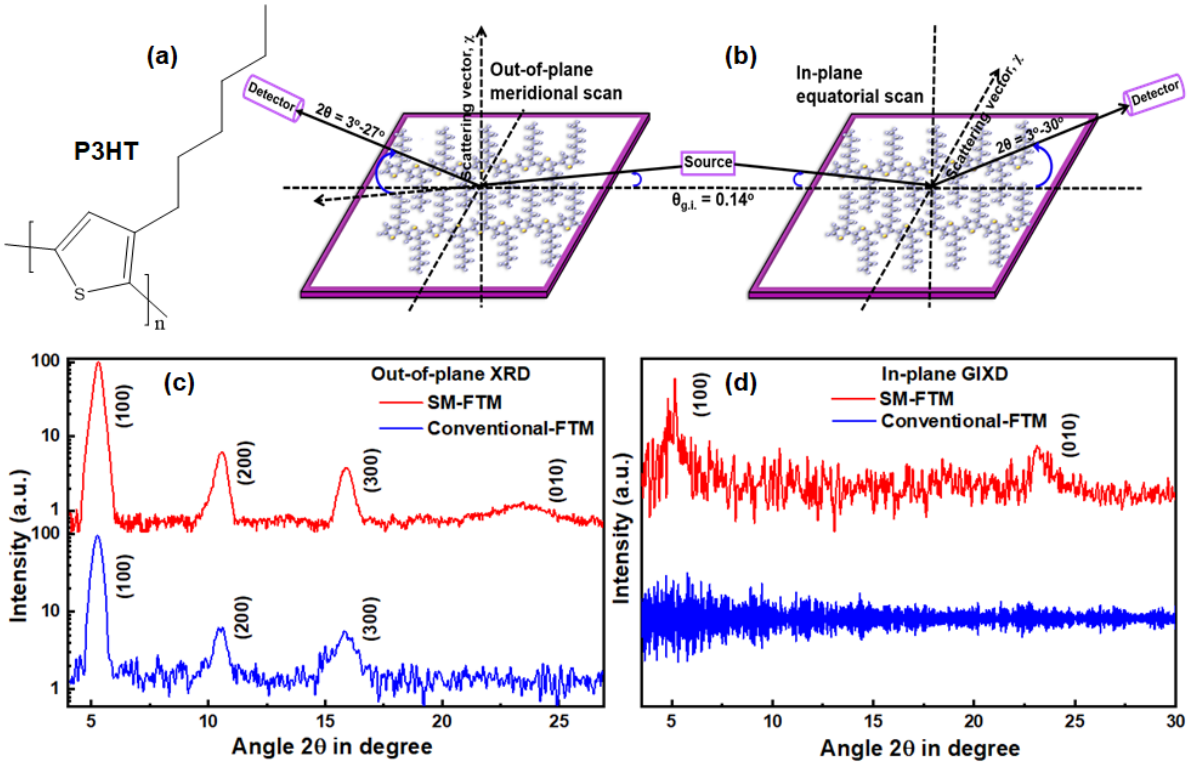

Figure 5.2 (a) Chemical structure of P3HT, (b) Schematic geometry of out-of-plane and in-plane GIXD measurements. (c, d) Out-of-plane and in-plane GIXD patterns of P3HT thin films prepared by conventional and subphase modified FTM.

the P3HT films is dominated by 'edge-on' stacking, then an out-of-plane meridional scan keeping the scattering vector (χ) almost perpendicular to the substrate surface should give us diffraction peaks corresponding to 'a'-axis only. As shown in Figure 5.2 (c), P3HT self-assembled through basic FTM shows only (*h*00) diffraction peaks, while film prepared using SM-FTM was found to show two sets of diffractions: three progressive (*h*00) peaks and a (010) peak. Thus, conventional-FTM films are assumed to have only 'edge-on' type molecular packing throughout the film structure, while SM-FTM films consist of both 'edge-on' and 'face-on' stacking. To further confirm our assumptions, we then characterize both films through in-plane grazing incidence X-ray diffraction (GIXD). Figure 5.2 (d) shows the in-plane GIXD patterns of the highly head-to-tail-coupled P3HT FTM films cast on single-oriented (001) Si-substrates. Surprisingly, conventional-FTM-made P3HT films show no diffraction peaks while we get both (100) and (010) diffraction peaks in the case

of SM-FTM films. As 'a'- and 'b'-axis intersect perpendicularly and χ was positioned almost parallel to the substrate surface during this measurement, it has been confirmed that both 'edge-on' and 'face-on' type molecular arrangements dominate the macrostructure of P3HT films prepared through SM-FTM. But conventional-FTM films consist of only one dominating packing where the 'a'-axis is perpendicular to the film plane i.e., 'edge-on'. Owing to weak Van der Waal's interactions between adjacent CP molecules, orientation and relative spacing highly influence molecular wavefunction overlap. As grain boundaries resist carrier delocalization, large coherence length can improve charge career mobility overwhelming the boundary effect. For qualitative analysis of the relative orientation and spacing between proximate molecules, the average coherence length (L_c), i.e., average crystal size, was estimated from the (100) peak using the Scherrer formula [109]. The interplanar spacings d_{100} (i.e., alkyl side-chain stacking distance) are found to be 16.8Å and 16.7Å for conventional-FTM and SM-FTM films, respectively and d_{010} (i.e., π-π stacking distance) is ~3.79Å for SM-FTM films which are congruous with theoretical models as well as previous experiments [101,158]. So, from the L_c values as summarized in Table 5.1, the average no. of Bragg's plane along the (*h*00) direction is estimated to be 14 and 13 for them. Here, we have ignored the peak broadening due to lattice distortion as we didn't get multiple orders of reflections in all the polymer films thus, we can't easily separate the two contributions, size and strain. While along (010) direction in a 'face-on' type molecular arrangement, on average 14 lamellas are found to be stacked together in SM-FTM films. The difference in d-spacing along the a-axis can be attributed to the degree of interdigitation and the tilting of polymer backbones across the c-axis. On the other hand, the presence of DBSA molecules at the solution-liquid interface facilitates some of the P3HT backbones which are close proximate to the interface, to self-assemble in a 'face-on' type packing, as schematically shown in Figure 5.1 (b). Interestingly, in oriented domains 'edge-on' and

Table 5.1 Findings of out-of-plane XRD analysis.

Sample (P3HT films)	Average d_{h00} in nm	Coherence length along (h00) in nm	Average no. of Bragg's plane (h00)	Average d_{0h0} in nm	Coherence length along (0h0) in nm	Average no. of Bragg's plane (0h0)
conventional-FTM	1.68	22.6	14	--	--	--
SM-FTM	1.67	20.7	13	0.38	5.0	14

'face-on' packing is almost same in SM-FTM films in terms of no. of Bragg's plane stacked together. So, this type of molecular arrangement is expected to enhance out-of-plane mobility by overwhelming microcrystalline perturbation-led resistances.

To further analyze these two types of distinct molecular packing present in the oriented crystalline zones, P3HT films were studied through HR-TEM at 200 kV energy and low irradiation level minimizing the polymer damage. In bright-field mode, an objective aperture cuts off the scattered electrons from the highly diffracting crystalline domains, which causes a slightly darker appearance of crystalline regions as compared to non-diffracting amorphous zones. In Figures 5.3 (a) & (d), at slightly lower magnification, although polymer backbone arrangement is not directly visualized, alternating dark and bright regions representing crystalline and amorphous zones are clearly noticeable in both the films. To probe different packing and periodicity, selected area electron diffraction (SAED) patterns were recorded centering on this region of interest. As shown in Figures 5.3 (c) & (f), the conventional-FTM film contains two (0*kl*) reflections representing 'edge-on' domination, while SM-FTM film shows a set of Scherrer rings having different intensities. The presence of (020), (0*kl*), and some (*hkl*) reflections evidenced the coexistence of "face-on" and "edge-on" type molecular packing with different periodicity

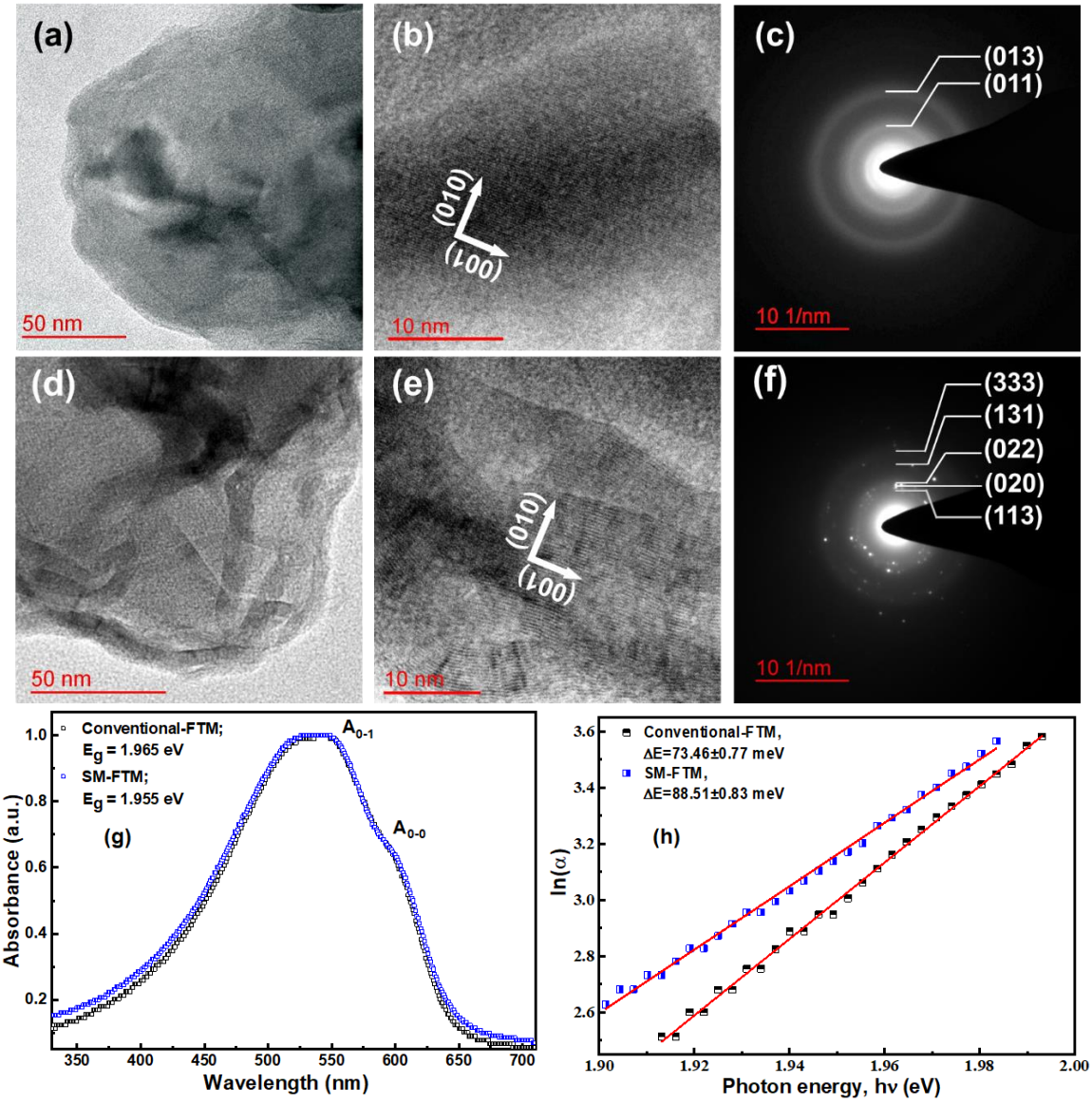

Figure 5.3 HR-TEM images and corresponding SAED patterns of conventional-FTM films (a-c) and SM-FTM films (d-f). Non-polarised optical absorption spectra (g) and corresponding low-energy absorption line-shape analysis (h) for both conventional-FTM and SM-FTM films.

in the SM-FTM film interior [54,164].

As the electron beam traverse parallels to P3HT backbones, the 2D projections of local molecular orientation at higher magnification can also provide detailed information regarding packing defects, chain fold, lattice bending, and lattice parameter fluctuations. As shown in Figure 5.3 (b), conventional-FTM films show larger domains of 'edge-on' stacking with fewer defects, as the forces acting at the liquid-solution interface help to

enlarge the average coherence length in an edge-on stacking only. But, in SM-FTM, dominating interaction between P3HT side-chains and long alkyl chains of sulfonic acid causes the fold of some P3HT backbones to attain a face-on type arrangement. In this folding process, many cumulative and non-cumulative disorders manifest in the crystal structure of SM-FTM films and it can be seen in Figure 5.3 (e). The periodic contrast modulation in bright field images represents the succession of electron-rich polythiophene backbones having intervals equivalent to the π-π stacking distance. Owing to the high alkyl side-chain density, flexible P3HT backbones balance any change in the acting forces during film formation by adopting many microstructural defects which are prominent in bright field HR-TEM images.

Next, to examine the effect of these two types of molecular arrangement on the macroscopic electronic band structures, we have recorded nonpolarized UV-vis absorption spectra at room temperature, shown in Figure 5.3 (g). As described by F. C. Spano, [165] the P3HT absorption spectra contain some peaks at the lower energy side that arises due to electronic transitions between states related to the π-stacked crystalline domains, while a broad tailing at the higher energy side appears due to transitions between intraband states having an amorphous origin. Among the crystalline contribution in the electronic absorption spectra, two peaks located at ~600 nm and 550 nm are assigned to the 0-0 and 0-1 transitions, respectively [166]. Now, considering the 0-0 electronic transition for P3HT a direct allowed type, the lowest optical gaps are found to be almost similar in both types of films. Thus, we can conclude that ‘edge-on’ and ‘face-on’ type molecular arrangements do not cause any significant change in the regular unpolarized optical absorption spectra. However, the transformation process involved in ‘edge-on’ to ‘face-on’ conversion introduces many microscopic perturbations that cause the Urbach type exponential tailing of the absorption band edge [92]. Thus, to quantify the quantum

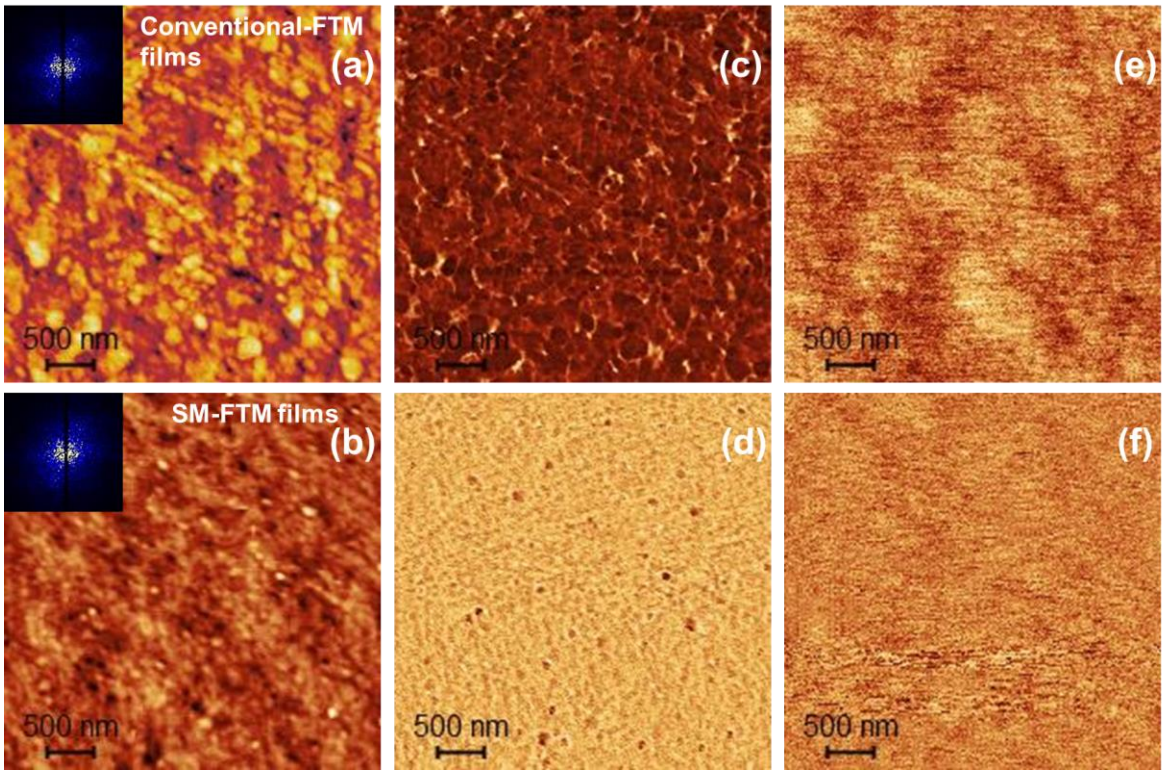

Figure 5.4 Evolution of surface topography in both films has been studied through AFM height profile (a, b), Phase profile (c, d) and work-function mapping (e, f), respectively.

mechanical penetration of localized traps into the optical gap, we have analyzed the absorption line shape in the lowest energy 0-0 transition region using the standard Urbach rule [112], equation 3.4. As shown in Figure 5.3 (h), the $\ln(\alpha)\ vs\ photon\ energy$ plot yields that Urbach energy, E_U $(= K_B T/\sigma_T)$ is higher in SM-FTM films, 88.51 meV compared to conventional-FTM films, 73.46 meV. Thus, the excitonic delocalization over the bc-plane in SM-FTM films will get more affected by these phonon fields, which is also evidenced by bright field HR-TEM images and they should reflect in the device performances.

As the inner microstructural properties mediate to the surface through the evolution of roughness topography, atomic force microscopy (AFM) has been employed in non-contact tapping mode to study the surfaces of both films. The AFM height profile, phase images and corresponding work function mapping are shown in Figure 5.4 (a-f). It can be seen

from the 2D Fast Fourier transformation (FFT) of AFM height profiles, as shown in the inset of Figure 5.4 (a, b), that the general perspective of the surface texture is isotropic, which is also clear from phase images [Figure 5.4 (c, d)]. The normalized probability density functions related to asperity heights follow a Gaussian-type distribution for both films. After that, analyzing the height profiles through the Gwyddion software, it has been found that SM-FTM film is smoother one having RMS roughness ($\boldsymbol{R_{rms}}$) ~0.98 nm, compared to ~1.47 nm in the conventional case.

While 'face-on' domination near the solution-liquid interface yields both globally and locally the smoothest surface. It is very promising to create a proper interface with the metal electrodes to facilitate easy charge injection and collection that will momentarily improve the overall device performance. After that, the topological evolution of work functions on film surfaces due to different processing conditions has been investigated through Kelvin probe force microscopy (KPFM) in amplitude modulation mode. Through electrostatic interaction between film surface and conducting AFM tip, KPFM reconstructs the film surface potential in real-time, as shown in Figure 5.4 (e, f). The surface potential topography for both films was found to follow a Gaussian distribution while the contact potential difference, V_{CPD} is greater for SM-FTM film as compared to conventional-FTM film. This is because it is easy to depart electrons from the peaks, if the sample surface is a rough one, the effective work function decreases. On the other hand, if the sample surface is a smoother one, the atoms become more densely packed on the surface, thus increasing the effective V_{CPD} [167].

5.2.2. Electrical and charge transport study

To study the effect of polymer chain conformations, degree of crystalline coherence, and interfacial microstructures on the out-of-plane charge transport, multiple conventional

Schottky barrier diodes (SBDs) were fabricated in a sandwiched structure of ITO/P3HT/AlO_X/Al as shown in the inset of Figure 5.5 (a). Conventional OSDs consist of an OSC sandwiched between two Ohmic and Schottky contacts and spontaneous charge transfers are energetically favorable for the ohmic contact, while the Schottky contact blocks it. Therefore, in a hole-only SBD, current will flow in one direction only (under forward bias) minimizing the switching time, and that is advantageous for fabricating high-performing devices like fast photo-detectors, etc. Now, from KPFM measurement, the work functions (φ_s) was found to be 4.596 eV and 4.595 eV for SM-FTM and conventional-FTM films, respectively. So, we have chosen ITO ($\varphi_m = 4.7\ eV$) and Al ($\varphi_m = 4.08\ eV$) for ohmic and Schottky contacts, [153] respectively, while a 10 nm AlOx layer was used to enhance the effective rectification ratio (RR) as optimized by Nikita et al. [81] The non-linear current density-voltage (J-V) characteristics as shown in Figure 5.5 (a) confirms the formation of rectifying Schottky contacts between Al/AlOx and P3HT. To elucidate this asymmetric J-V relation, we have used the thermionic emission model as following [153], equation 3.5. The ideality factor, η and reverse saturation current density, J_0 has been determined from the slope and intercept of semi-logarithmic J-V plot (calculated from the linear part). The interfacial Schottky barrier height, φ_B which have a profound effect on RR has been evaluated using reverse saturation current density and all the estimated electrical parameters have been summarized in Table 5.2. As high rectification ratio is one of the key requirements for industrial-level diode fabrication, we have improved our film fabrication technique with respect to RR and also compared our best result with currently available reports (Table 5.3). Initially, the required volume of DBSA to provide a proper density of long alkyl chains at the interface has been optimized (1.3%) as shown in Figure 5.5 (b). It is clearly observable that, while increasing the DBSA volume beyond the optimum 1.3%, RR doesn't vary significantly. This is justified because

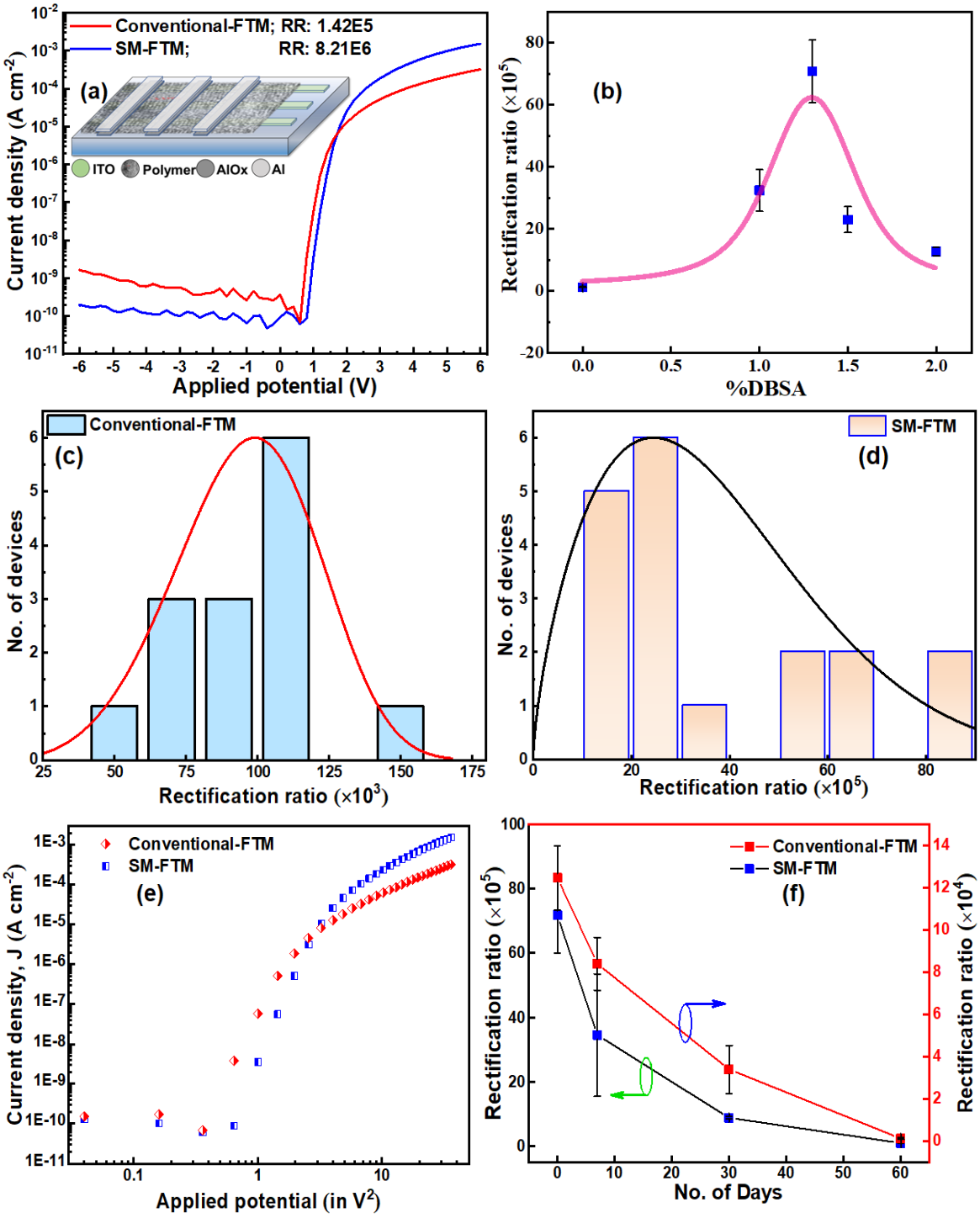

Figure 5.5 (a) J-V characteristics of both P3HT films, (b) Optimization of DBSA percentage in terms of RR, (c, d) histogram of RR measured in many devices, (e) corresponding J-V^2 plot, (f) stability study of SBDs.

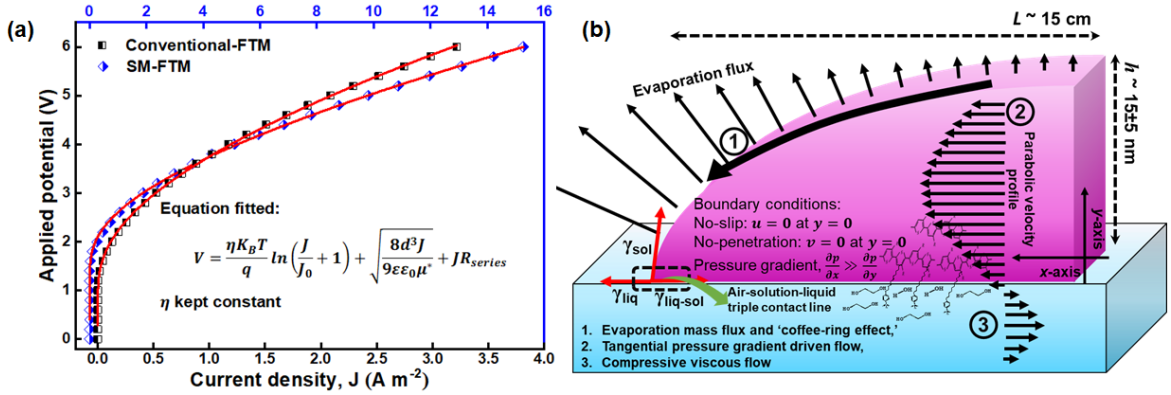

Figure 5.6 (a) Forward bias J-V characteristics fitting to estimate the overall Ohmic loss, (b) Schematic illustration of FTM dynamics in the leading edge of ribbon-shaped FTM.

Table 5.2 Electrical parameters analyzed for both conventional-FTM and SM-FTM films in SBD architecture.

Electrical parameters	conventional-FTM film		SM-FTM film	
	Regional linear fit	J-V full fit	Regional linear fit	J-V full fit
Ideality factor, η	3.16 ± 5.5%		2.68 ± 7.6%	
Saturation current density, J_0 (μA/cm^2)	3.3 ± 15.1%	2.3×10^{-4} ± 10.9%	0.34 ± 9.3%	0.33×10^{-4} ± 1.8%
Schottky barrier height, φ_b (meV)	103.5 ± 7.31%	470.0 ± 2.1%	161.8 ± 7.4%	520.0 ± 1.2%
Intrinsic mobility, μ (cm^2 V^{-1} s^{-1})	3.6×10^{-5} ± 1.8%		5.6×10^{-5} ± 2.9%	
Effective mobility, μ^* (cm^2 V^{-1} s^{-1})		9.0×10^{-7} ± 10.9%		40.5×10^{-7} ± 4.0%
Series resistance, R_{series} (Ω cm^2)		2485.3 ± 12.5%		238.7 ± 1.2%

only a limited amount of P3HT molecules face the DBSA alkyl chains which are adjacent to the solution-liquid interface and DBSA volume increment doesn't significantly changethe fraction of 'face-on' type molecular stacking. To standardize our film fabrication technique, multiple devices have been fabricated by stamping the films from similar positions on the ribbon-shaped FTM films and their corresponding RR has been demonstrated in Figure 5.5 (c, d). Furthermore, the air stability of our devices has also been studied as illustrated in Figure 5.5 (f). As the P3HT layer is sandwiched between two

contacts and properly annealed, the devices show pretty good electrical performance during initial few days (relative humidity ~20-30%) and then RR decreases for both types of devices. But, even after 60 days, both type of diodes still retains RR ~10^5 and ~10^3 (for SM-FTM and conventional-FTM films, respectively), which can be improved further by adding a simple protective layer. Further to study the dependence of vertical charge transport on the interfacial molecular arrangement, we have plotted the J-V^2 graph [Figure 5.5 (e)] taking the best device results of each kind and then the intrinsic mobility (μ) has been determined using the well-known Mott-Gurney relation [153], equation 3.6. The effective channel length, *d* that refers to the total film thickness, has been taken as 225 nm for 15 layers (~15 nm for 1 layer as studied through AFM step height). Now, the overall diode performance depends on two major parameters: bulk charge carrier mobility (i.e., μ) and overall resistance [i.e., $R_{total} = R_c(\text{interfacial contact resistance}) + R_b(\text{bulk resistance})$]. At high forward bias, after filling all traps, current depends only on the injected holes in trap-free space charge limited region and thus μ evaluated from J-V^2 plot found to be highest for SM-FTM films (5.6×10^{-5} ± 2.9%) is because of its particular molecular arrangement. Now, because of high degree of conformational freedom, backbone flexibility and weak Van der Waal coupling between neighboring molecules, P3HT self-assembly at air-liquid interface introduce many trap states in the film bulk. While the presence of unsaturated surface dangling bonds and thermal deposition of metal contacts causes interfacial traps. The effective contribution of these non-uniformly distributed trap states in the overall J-V response varies with applied bias. Thus, to quantify the effective charge carrier mobility, Schottky barrier height and the compound effect of defects and molecular arrangement, we have fitted the whole forward bias J-V characteristics [Figure 5.6 (a)] with the following analytical model equation [81],

Table 5.3 Summary of previously reported characteristic SBDs compared with our results.

Structure	Rectification ratio	Publication year
ITO/ZnO/Pentacene/Au [168]	3×10^3	2008
Au/PEDOT:PSS/P3HT/Al [169]	3×10^4	2009
Cu/CuTCNQ/Pentacene/Al [170]	2×10^6	2010
Cu/PTAA/Ag [171]	$\sim10^5$	2011
Pt/InGaZnO/Al [172]	2.2×10^4	2016
Au/PFBT/Pentacene/Al [154]	1.05×10^7	2016
Cr/Au/C_{16}IDT-BT/MoO_3/Ag [173]	$>10^6$	2017
ITO/P3HT(fiber)/Al [153]	$\sim10^3$	2017
Au/P3HT(Spincoat)/AlOx/Al [81]	1.11×10^6	2019
Pt/P3HT-PMMA/IGZO/ITO [149]	$\sim10^4$	2019
Au/PFBT/P3HT/Al [155]	$\sim10^6$	2021
ITO/P3HT(conventional-FTM)/AlOx/Al	**1.42×10^5**	**This work**
ITO/P3HT(SM-FTM)/AlOx/Al	**0.82×10^7**	**This work**

$$V = \frac{\eta K_B T}{q} ln\left(\frac{J}{J_0} + 1\right) + \sqrt{\frac{8d^3 J}{9\varepsilon\varepsilon_0 \mu^*}} + JR_{series} \tag{5.1}$$

Here, R_{series} (in Ω cm^2) represents the ohmic loss across the whole device architecture and μ_h^* is the effective hole mobility. It has been found that, the overall Ohmic loss, R_{series} decreased by one order of magnitude in diodes made of SM-FTM films, while the effective mobility, μ^* enhanced ~4 times as compared to conventional-FTM films. Thus, in spite of having a greater density of bulk defects as found from Urbach energy quantification, active layer prepared through SM-FTM makes a better device. This better performance can be accounted for two reasons: first, highly smooth surface topography facilitates easy charge transfer delocalizing the hole wavefunction through metal-semiconductor junction [106] and secondly, higher degree of orbital overlap in 'face-on' type molecular assembly provides a low-resistive path for the charge carriers. Nonetheless, to probe this

microstructural evolution of FTM films along the out-of-plane direction that profoundly affects the SBD performance, we have demonstrated the molecular rearrangement mechanism within the framework of an analytical model developed using lubrication theory as described below.

5.2.3. Theoretical interpretation of SM-FTM

Melts and solutions of polymers having sufficiently high molecular weight usually show non-Newtonian shear-thinning behavior when sheared, as the disentanglement of randomly oriented molecular chains causes viscosity to drop [174]. We are using a polymer with M_w: 50,000-75,000 and a relatively low concentration solution (10 mg/ml). Further, before spreading the polymer solution over a high surface energy liquid bed, it has been heated at 60 ^oC for 1 hour to erase all the thermal history and aggregation, which yields complete disentanglement of polymer chains. In this state, the viscosity of the chloroform solution of rr-P3HT doesn't depend on the shear rate, which means they behave like a Newtonian fluid [94]. Thus, when this polymer solution is subjected to tangential stress caused by surface tension gradient, they encounter macroscopic as well as microscopic deformation through conformational changes and viscoelastic flows. The direction and strength of these viscoelastic flows along with the intermolecular π-π interaction, govern the self-assembly and molecular stacking at air-liquid interface. Thus, to analyze the polymer spreading and the effect of DBSA present at air-liquid interface, we have solved the velocity profile of thin-liquid film flow using lubrication theory and steady-state Navier-Stokes equations [175–177].

For ribbon shaped-FTM, we are using a parallel plate Teflon slider with a rectangular channel of length~1 cm and width~2 cm as shown in Figure 5.1 (a), which allows a two-dimensional planar fluid flow due to surface pressure gradient. Interestingly, this 1 cm long rectangular channel proved to be sufficient lengthscale to form a quasi-steady fully

developed flow, [175] where height 'h' is along y-lengthscale and length, L along x-lengthscale. Figure 5.6 (b) shows the geometry and coordinate system used to establish this model. In our system, $h\sim 15 \pm 5\ nm$ and $L\sim 20\ cm$ (i.e., ratio, $\epsilon = \frac{h}{L}\sim 10^{-7}$), thus, the pressure gradient, Δp along $y \ll \Delta p$ along x (i.e., $\frac{\partial p}{\partial y} \ll \frac{\partial p}{\partial x}$). If film thickness, h changes with respect to position, x and time, t then we can define a variable to access this combined spatiotemporal change in film thickness as, $F = y - h(x,t)$; while for a flat interface, $y = h(x,t)$. As hydrophobic chloroform and hydrophilic liquid bed are immiscible, polymer solution can't penetrate into the liquid substrate; this gives the 'no-penetration' boundary condition, i.e., y-velocity, $v = 0$ at $y = 0$. Further, due to dipole-dipole interaction between chloroform and Glycerol, the very first layer of the polymer solution will try to remain at rest by transferring its momentum to the lower liquid substrate which is also at rest. Thus, there will be zero relative velocity between the polymer solution and lower liquid bed at the liquid-solution interface, which gives the 'no-slip' boundary condition, i.e., x-velocity, $u = 0$ at $y = 0$.

Now, as there only one body force corresponding to evaporation-led endothermic divergent mass flux is dominating towards the x-direction, [124] while the gravity force working along the vertical y-direction, from Navier-Stokes equation, x-momentum and y-momentum equations will be,

$$0 = -\frac{\partial p}{\partial x} + \frac{\partial^2 u}{\partial y^2} + \frac{{l_c}^2 \epsilon^2}{\mu u_c} J_s \tag{5.2}$$

$$0 = \frac{\partial p}{\partial y} + \frac{\epsilon^3 {l_c}^2}{\mu u_c} \rho g \tag{5.3}$$

where ρ, μ, g, and J_s represent the liquid density, viscosity, acceleration of gravity, and evaporation flux respectively [97]. The characteristic variables, u_c and l_c are representing

velocity and length which are being used for the non-dimensionalization of thin-film equations. Then, the tangential force balance requires that,

$$\frac{\partial u}{\partial y} = \frac{\epsilon}{C_a}\widetilde{\nabla}\sigma \tag{5.4}$$

where $\widetilde{\nabla} = \frac{\partial}{\partial x} + \frac{\partial h}{\partial x}\frac{\partial}{\partial y}$; σ corresponds to the surface tension coefficient at any x, and C_a represents the capillary number, $C_a = \frac{\mu u_c}{\sigma_0}$, σ_0 is the reference surface tension coefficient of polymer solution at $x = 0$. After that, from balancing the normal forces, we get

$$p_s - p_0 = -\frac{\epsilon^3}{C_a}\sigma\frac{\partial^2 h}{\partial x^2} + p_{ex} \tag{5.5}$$

Here, $p_s =$ pressure at the air-solution interface i.e., at $y = h$; $p_0 =$ pressure at the liquid-solution interface, i.e., at $y = 0$; and $p_{ex} =$ excess pressure or disjoining pressure. Now, in our case, as the surface tension gradient is the dominating force, it can be approximated that, $\frac{\epsilon}{C_a} \sim 1$ i.e., $u_c \sim \frac{\epsilon\sigma_0}{\mu}$. Again, $\frac{\epsilon^3}{C_a}\sigma\frac{\partial^2 h}{\partial x^2} \to 0$ as $\epsilon \sim 10^{-7}$; therefore, from the normal force balance, we get

$$p_s - p_0 = p_{ex} \tag{5.6}$$

For the case of simple Glycerol-water mixture, there present a polar interaction only at the solution-liquid interface, so, we can take $p_{ex} \sim 0$. Thus, solving the y-momentum equation, we get

$$p = p_0 + k(h - y) \tag{5.7}$$

where $k = \frac{\rho g \epsilon^2 {l_c}^2}{\sigma_0}$, is a constant while mass conservation is maintained. After that, using the 'no-slip' boundary condition and taking a 'non-deforming' air-solution interface (that means, $\frac{\partial u}{\partial y} = 0$ at $y = h$), the tangential stress balance and x-momentum equation yields the following,

$$u = \frac{k\frac{\partial \sigma}{\partial x}\left(\frac{y^2}{2} - yh\right)}{k(y-h) - \frac{\partial \sigma}{\partial y}} \tag{5.8}$$

Now, for the 1.3% DBSA mixed hydrophilic liquid mixture, there exists a LW type induced dipole-induced dipole interaction due to the electron cloud localization, acid-base type polar interaction, and finally, a dominant interaction between the polymer alkyl side-chain and the long hydrophobic tail of DBSA. Thus, at the super end stage, when the droplet of the polymer solution flattens down so much that these Van der Waals forces become significant and we can't neglect the effect of p_{ex} $(= \frac{A}{6\pi h^3})$. Then, the velocity profile will get modified as following,

$$u = \frac{\left(k - \frac{A}{2\pi h^4}\right)\frac{\partial \sigma}{\partial x}\left(\frac{y^2}{2} - yh\right)}{\left(k - \frac{A}{2\pi h^4}\right)(y-h) - \frac{\partial \sigma}{\partial y}} \tag{5.9}$$

where A represents the Hamaker constant [178]. So, mixing an optimum amount of DBSA into the conventional hydrophilic liquid bed reduces the x-component of the velocity profile by enhancing the Van der Waals forces at the liquid-solution interface and reducing the effective surface tension gradient. Thus, from equations (5.8) and (5.9), it is clear that, surface tension as a driving force creates a pressure difference. Although, the surface tension gradient is acting on the interface, but the differential pressure eventually controls the flow and its velocity profile is found to be parabolic in nature. This tangential stress driven flow is linked with a compressive viscous flow of hydrophilic liquid bed at the solution-liquid interface which acts opposite to the solution flow. Apart from this, the divergent evaporation flux which is highest at the contact line needs a fluid flow from the interior to replenish the mass loss. This flow causes solutal deposition near the progressing triple contact line (air-solution-liquid) [96,97]. Moreover, due to the presence of a finite air-solution interface, a resistive viscous force at the solution-liquid interface, and repulsive interaction between the hydrophilic -OH groups and non-polar hydrophobic alkyl side-

chains assist the rr-P3HT backbones to self-assemble in an edge-on dominated molecular stacking. But when we neutralize the repulsive interaction up to an extend by introducing DBSA molecules whose long hydrophobic tail is exposed towards the air/solution, rr-P3HT backbones start attaining a 'face-on' stacking.

5.3.Conclusions

In conclusion, we have successfully developed a novel film fabrication technique (called SM-FTM) by improvising the ribbon-shaped FTM. In this technique, the macromolecular arrangement at solution-liquid interface can be controlled by tuning the polymer-liquid substrate interaction. SM-FTM includes key advantages (similar to conventional ribbon FTM) like large-area and homogeneous film formation, layer-by-layer coating capability, compatibility with various substrates having smooth surface etc. along with control over molecular packing. We further demonstrated the dynamics of polymer solution spreading over air-liquid interface and the effect of DBSA-polymer interaction through a simple model based on lubrication theory and thin-liquid film flow kinetics. This model predicts that the introduction of DBSA reduces the leading-edge velocity (u) and facilitates 'face-on' type molecular packing at the interface, which is in good agreement with the experimental observations. The in-plane and out-of-plane GIXD patterns evidenced that both 'edge-on' and 'face-on' type molecular arrangements are found in SM-FTM films, while only 'edge-on' dominates the conventional-FTM film microstructure, which also justified by bright field HR-TEM images. Next, the molecular rearrangement process has been found to be ineffective in changing the overall band structure except for the Urbach type exponential tailing of the absorption band edge. The AFM, work function mapping, and contact angle measurements show that SM-FTM films are locally the smoothest ones, and that is desirable for injection-efficient contact formation. Finally, via implementing an interfacial engineering approach, the state-of-the-art rectification ratios of ~10^7 in SBDs

and almost 400% increment in the effective out-of-plane mobility as compared to the conventional FTM films have been achieved. Thus, SM-FTM opens a new direction of material processing to engineer high-performing out-of-plane devices along with the planar OFET structure through conventional FTM.